Fast Dynamic Color Switching in Temperature-Responsive Plasmonic Films

*Tao Ding, Christian Rüttiger, Xuezhi Zheng, Felix Benz, Hamid Ohadi, Guy A. E. Vandenbosch, Victor V. Moshchalkov, Markus Gallei, and Jeremy J. Baumberg**

Over the last two decades tremendous effort has been devoted toward plasmonically active materials for various applications in nanophotonic devices, bio-/chemical-sensing, metamaterials, photocatalysis, solar cells, and water splitting.[1–3] However, it remains a grand challenge to realize dynamic and reversible tuning of plasmons with large spectral shifts, which can be applied in large-area wallpapers and video walls, as well as sensors. Previous attempts to realize such a dynamic and reversible tuning used liquid crystals,[4,5] phase-change materials, DNA origami,[6–8] mechanical stretching,[9,10] stimuli-responsive polymers,[11–14] and electric fields.[15,16] However, either the tuning range was very small (<50 nm) or the plasmonic nanostructures were poorly defined (random aggregates), which hinders in-depth understanding and practical applications. In addition, tuning rates have been rather slow, on the timescale of seconds.

Placing a nanoobject in an optical cavity enhances the scattering cross section if the object is located at an antinode of the optical field. Modulating the resonant modes by changing the cavity length then changes this scattering cross section. Since plasmonic scatterers possess optical cross sections much larger than their geometrical cross section, using them as such nanoobjects can create efficient scattering surfaces (metasurfaces). A simple way to modulate plasmonic scattering is thus to change the length of the cavity in which they are put;[17,18] however, it has been hard to achieve this reversibly at high speed over large areas.

Poly[*N*-isopropylacrylamide] (pNIPAM) is a temperature-responsive polymer that has long been used in actuation, membranes, biosensing, tissue engineering, and drug delivery.[19,20] Due to its strong volume shrinkage (up to 90%) when the temperature rises above a critical hydration temperature (T_c) and its full reversibility across this phase transition, pNIPAM has been utilized to tune plasmons in Au/Ag nanoparticles (NPs) and nanorods.[21–27] However, because these plasmonic assemblies are either randomly decorated around the surface of pNIPAM microgels or aggregates with undefined number of particles and configurations, it is hard to understand the physics of the mixture of different plasmonic constructs properly. Moreover, it takes time for water to diffuse inside the microgels to fully swell them, thus the speed of volume changes has been relatively slow (typically a few seconds).

Here, we graft pNIPAM layers (d = 70 nm thick) onto Au mirror by applying surface-initiated atom transfer radical polymerization (SI-ATRP) protocols, and place scattering Au NPs on top. By utilizing the phase transition of the pNIPAM, the separation between Au NP and Au film is widely tunable, thereby leading to a dynamic and reversible plasmon tuning system based on modulating the resonant modes. The resulting films exhibit strong color changes, are simple to fabricate, can be flexible, are low cost, can easily scale to large areas, and respond faster than video rates. In addition, the plasmonic nanoparticles can also be optically irradiated to locally switch the surrounding pNIPAM layers, creating video-rate all-optical switching over large areas.

The Au mirrors are deposited via electron beam evaporation with roughness controlled below 1.5 ± 0.5 nm.[28] The pNIPAM films are then prepared on these Au films by SI-ATRP (**Figure 1**, Experimental Section).[29] The thickness of the as-grown dry pNIPAM films is determined to be 67 ± 1 nm via ellipsometry (Figure S1, Supporting Information). The molecular weight estimated from the free pNIPAM synthesized under the same condition is 26.3 kDa as determined by size-exclusion chromatography. The transition temperature of this pNIPAM film determined through contact angle measurement is around 30 °C (Figure S2, Supporting Information). This value is slightly lower than the normal lower critical solution temperature (LCST) (32 °C) of pNIPAM mainly because of the residue Cu^{2+} salts and polar end groups introduced during the ATRP process. The D = 100 nm diameter Au NPs (from BBI Solutions with 10% monodispersity, Figure S3, Supporting Information) deposited on the films from solution appear slightly embedded inside the pNIPAM brushes as seen in scanning electron microscopy (SEM) images (inset Figure 1). Nanoparticle densities are varied up to 1 nanoparticle μm^{-2} to ensure that there is minimal coupling between nanoparticles, while the total scattering is maximized. Though this Au NP on mirror (NPoM) is related to the recent advances in small-gap constructs,[22] here the gap remains larger than the radius, reducing the plasmonic

Dr. T. Ding, Dr. X. Zheng, F. Benz, Dr. H. Ohadi, Prof. J. J. Baumberg
Nanophotonics Centre
Cavendish Laboratory
University of Cambridge
Cambridge CB3 0HE, UK
E-mail: jjb12@cam.ac.uk
C. Rüttiger, Dr. M. Gallei
Ernst-Berl Institut für Technische und Makromolekulare Chemie
Technische Universität Darmstadt
Alarich-Weiss-Straße 4, 64287 Darmstadt, Germany
Dr. X. Zheng, Prof. G. A. E. Vandenbosch
Department of Electrical Engineering (ESAT-TELEMIC)
KU Leuven 3001, Belgium
Prof. V. V. Moshchalkov
Institute for Nanoscale Physics and Chemistry (INPAC)
KU Leuven 3001, Belgium

DOI: 10.1002/adom.201600094

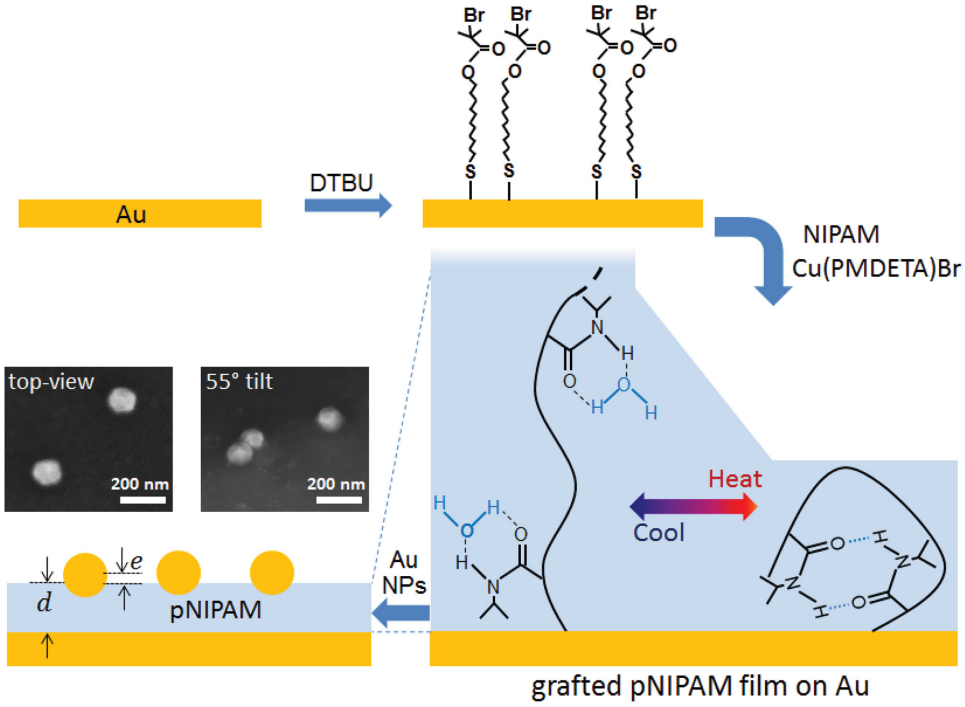

Figure 1. SI-ATRP polymerization of NIPAM spacer film on Au substrate (see the Experimental Section) and fabrication of the tunable scattering construct by deposition of Au NPs. Insets are SEM images of the Au NPs on the films observed from different angles.

coupling to the image nanoparticle in the mirror, but interferometrically interacting with the mirror (as modeled below).

The samples are immersed in water and capped with a coverslip for dark-field imaging, with incandescent white light incident at 60° to the normal, and collected over ±20° around normal incidence. Initially, a hot stage controls the temperature of the water. These Au NPoM films show relatively intense scattering-based color, which changes from green at 25 °C to orange at 35 °C (**Figure 2**a,b), clearly visible to the naked eye. Tracking the scattering spectra of a single NPoM during cycling of the liquid temperature between 25 °C and 35 °C (Figure 2b,c, curves smoothed for clarity) reveals the disappearance of the p_2 mode at λ = 550 nm followed by the appearance of a new p_0 mode in the infrared which blueshifts from 1000 nm into the visible, saturating at 630 nm. Upon cooling, these spectral shifts exactly reverse. The color can reversibly change back and forth many times with excellent reproducibility (Figure 2e) and can be stably tuned when holding the sample at intermediate temperatures (Figure 2c). The spectral shifts of the labeled modes (p_i) are extracted and summarized in Figure 2f, showing an additional weak p_1 mode which appears only transiently. The largest scattering intensity per individual NPoM is currently 0.2% for our illumination and limited by their optical cross section, although this can be increased by using closely-spaced dimers and trimers.[30] The $\Delta\lambda \approx$400 nm spectral shift obtained on switching (for the p_0 mode) is the largest for a reversible plasmonic construct yet recorded, and seen for NP films of many different diameters (samples prepared with D = 60, 80, or 100 nm NPs all show similar response differing mainly in the scattering strength). Each NPoM over the area shows the same dynamic tuning, though the initial and final colors vary slightly for different samples due to the slightly different pNIPAM thickness and the occasional presence of a rod-shaped or dimer of Au NPs (Figure S4, Supporting Information). We also measure the temporal evolution of the pNIPAM spacer using a thicker film capped with 100 nm NPoMs (Figure S5, Supporting Information). This allows us to track simultaneously several cavity modes, giving the optical path length and thus calibrating the separation of NP from the mirror (extracted from Equation S13, Supporting Information), and showing the significant nonlinear collapse in thickness during a heating cycle.

To understand the experimental results, we start by assuming that the Au NP can be modeled as a dipole $\boldsymbol{\mu}$ centered at position r_0 due to its small size with respect to the wavelength (**Figure 3**a). This dipole can be polarized in any direction, while its strength depends on the incident field $E_i(r_0)$ via (see the Supporting Information for full details)

$$\left\{\overline{z}_0(r_0,r_0;\omega)+\overline{z}_r(r_0,r_0;\omega)\right\}\mu(r_0)=E_i(r_0) \quad (1)$$

In the above equation, the tensor function $\overline{z}_0(r_0,r_0;\omega)$ represents the direct field contribution, while $\overline{z}_r(r_0,r_0;\omega)$ is the reflected field contribution mediated by the Au mirror underneath. Their sum $\overline{z}_t=\overline{z}_0+\overline{z}_r$ becomes small at certain wavelengths indicating resonances in the Au NP response. The field $E_i(r_0)$ combines both *s*- (TE) and *p*- (TM) polarized components (see Equations S11,S12, Supporting Information).

When the Au NP is more than 250 nm from the mirror, the combined response $\overline{z}_t$ has negligible contribution from the mirror, so the NP behaves as in free space (via $\overline{z}_0$) with single-particle plasmonic resonance ≈590 nm (Figure S6,

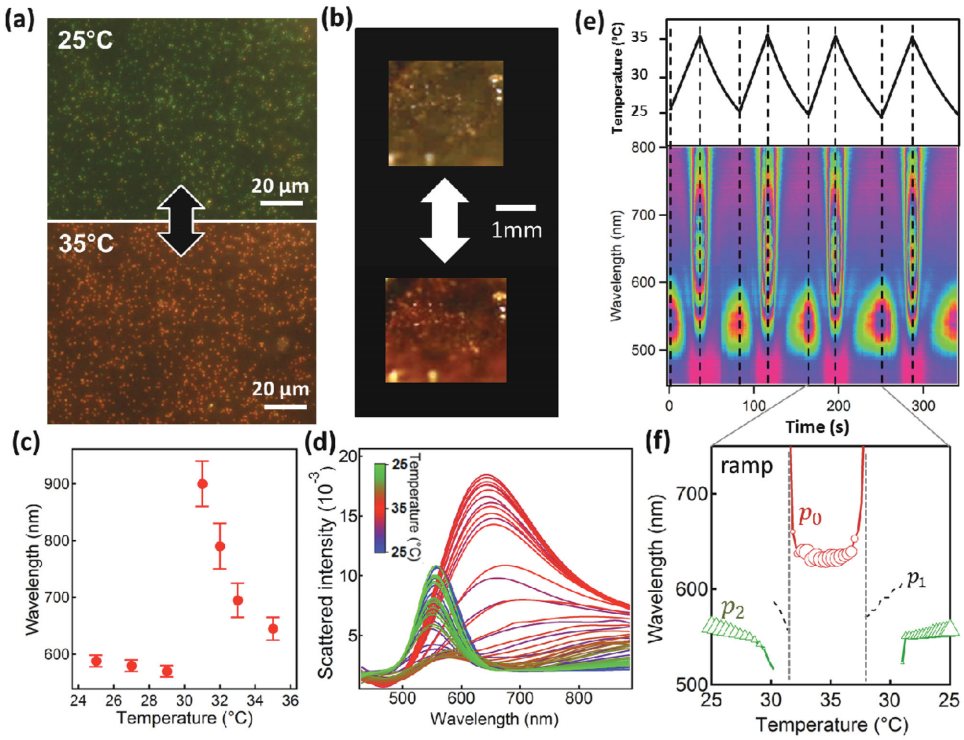

Figure 2. Thermal cycling of 100 nm Au NPoM with pNIPAM spacer. a,b) Directly observed color of the scattering image switches between 25 °C and 35 °C in a) dark-field microscope and b) to the naked eye. c) Peak spectral response wavelength as temperature slowly changed. d) Scattering spectra of a single Au NPoM as temperature is increased and reduced. e) Cycling of scattering spectra with time as temperature cycles. f) Extracted peak resonances shifting through one cycle of heating and cooling.

Supporting Information). On the other hand, when the Au NP is much closer (d < 100 nm), the contribution from the mirror is significant, with $\overline{z}_r$ comparable to $\overline{z}_0$ (Figure S7, Supporting Information). This plasmonically couples the Au NP plasmon, shifting it to longer wavelengths, mostly dominated by the vertically polarized components. Since the resonant form of the system is fully defined by the sum $\overline{z}_t$ regardless of incident angle, this resonance should always be observed. This scheme therefore promises good color performance over a wide viewing angle.

The practical performance shown in experiment can be recovered in numerical simulations. Calculations are based on gap sizes from 100 to 250 nm using a mixture of TE and TM light corresponding to the unpolarized light in experiments, and collecting the scattered power in a cone of 20°. When cold, the scattering angular half width (excluding higher angles >50°) is <15 nm, while in the hot state the angular shift is ten times smaller. The numerical results from our model (Figure 3b–d) capture very well the experimental spectra (Figure 2d and Figure S8, Supporting Information). The small dependence on incident angle theoretically predicted is seen for both the d = 100 nm (hot) and d = 250 nm (cold) cases (Figure 3c,d). We also find that poor plasmonic metals (e.g., Ni nanoparticles) in the visible gives a much smaller coupled scattering response (more than an order of magnitude smaller). Coupling effects here are thus a result of highly polarizable nanoparticles close to a highly polarizable surface, and this gives strong sensitivity to changes in gap spacing. While each construct can be reliably assembled onto the surface, on the other hand in the regime here their lateral spacing has little effect on the optical response, which means that many large-area coating techniques can be used to create them simply and cheaply. We also note that Al mirrors can be used in this interferometric regime, compatible with large-area fabrication.

The plasmonic NP resonance provides an optical route to actuate this color change, since the strong local field allows direct photothermal heating of the pNIPAM layer underneath. When a UV laser at 447 nm is used, as well as producing the spectral shifts it simultaneously photothermally degrades the polymer, and the shifts are not reversible (Figure S9, Supporting Information). By instead focusing a 637 nm laser onto an NPoM with resonance in the infrared, we can locally trigger it above T_c while the surrounding NPs are unaffected (**Figure 4**a,b). The spectra (filtering out laser light at shorter wavelengths) show no color shifts until laser powers of 120 µW focused to a 1 µm spot are applied, and then they shift in the same way as for global heating (Figure 4b) but stop in the infrared region (930 nm). This is because photothemal heating is locally confined around each Au NP (within a distance of 20 nm in bulk water). Cooling from the surrounding environment limits the temperature rise above the LCST of pNIPAM, and the fraction of the film that responds, and reducing the blueshift observed. Note that when the NPoM is cold, the resonant mode redshifts beyond our spectrometer window. When the laser is switched off, the NPoM rapidly recovers to the original spectrum, and these spectral changes can be repeatedly cycled (Figure 4c,d). Neither

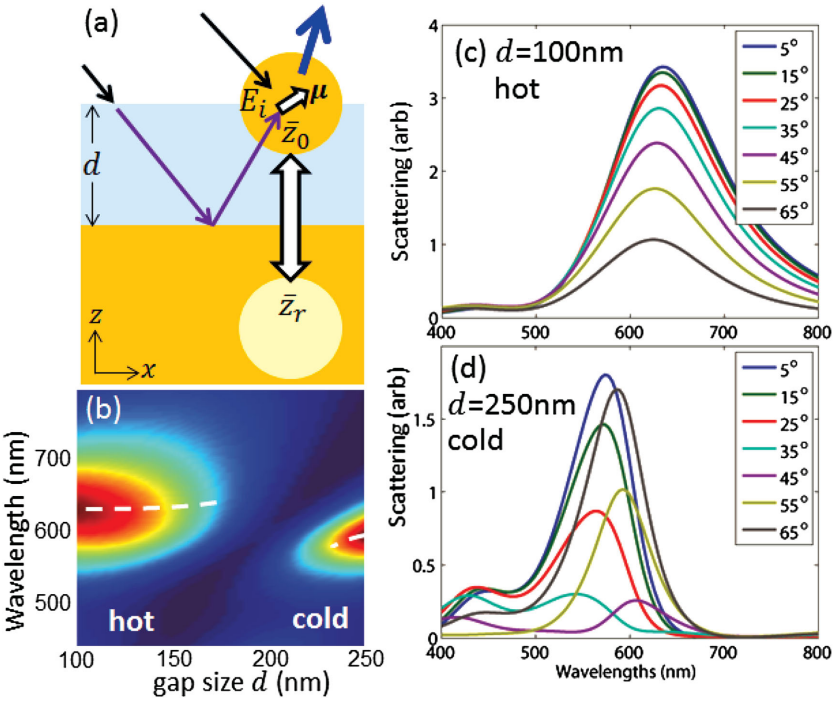

Figure 3. a) Schematic interference paths for scattering Fabry Perot cavity. b) Simulation spectra for 100 nm Au NP on pNIPAM solvated film, as it collapses from 250 to 100 nm when heated to 35 °C. Simulated scattering of Au NPoM with pNIPAM spacer thickness of c) 100 nm and d) 250 nm at different incident angles.

NP nor pNIPAM is damaged as the water inflates and deflates the film, at least for the hundreds of cycles applied here.

The blueshift observed appears instantaneously upon irradiation, which suggests that heat accumulation and the phase transition can be very fast at the nanoscale, compared to the typical bulk pNIPAM switching of seconds.[31,32] To measure the switching speed, we modulate the heating laser while integrating all of the infrared light scattered from a single NPoM on a fiber-coupled photomultiplier (Figure S10, Supporting Information). Upon turning on the laser, the scattering rises within 2 µs (Figure 4e), which is at the limit of our detection sensitivity. Similarly, the decay time also has this extremely fast response. The characteristic thermal times can be understood from the thermal conductivity and heat capacity of the 20 nm thick thermal layer of water around the NP which is heated, that yields predicted cooling time of <100 ns.[33] The intrinsic speed of the expulsion of water across several 100 nm during the phase transition has not previously been observed, and the NPoM construct here provides an ideal method to achieve this. By dividing the responsive pNIPAM material into ultrathin coatings below nanoparticles, the switching response thus becomes very fast. Although further understanding of the actuating speed and its relation with molecular pNIPAM molecular weight and packing density can be explored, we note that already large-area color-changing surfaces are produced here that can be modulated faster than video rates, and thus can be the basis for devices such as displays.

In conclusion, we have established a dynamic, ultrafast, and reversible plasmonic switching system based on the Au NPoM construct. The pNIPAM film between the Au NP and Au mirror acts as a nanoactuator to lift the NPs up and down, which shifts the plasmonic resonances of the resonator formed between mirror and scattering NP. The local nonlinear switching of the pNIPAM above T_c can be triggered either by heating or light. Such a reversible dynamic tuning system provides a new way to couple local changes in temperature, solvation, plasmonics and optical interference, thus opening up a range of optochemical explorations at the nanoscale. In addition, these ultrafast tuning surfaces can provide functionality (provided thin water layers are encapsulated) for low-cost large-area switching structural-color devices such as wallpapers, sensors, bandages, textiles, and displays.

Experimental Section

Fabrication of AuNPs on pNIPAM/Au Film: The Au mirrors were fabricated by depositing 50 nm Au films onto silicon wafers using ebeam evaporation (rate 1 Å s^{-1}, vacuum 5 × 10^{-6} mTorr) with 5 nm of Ti used as an adhesive layer. The gold films were UV irradiated (λ = 365 nm) for 1 h prior to immersion in the initiator solution to remove contaminating organics. The samples were then placed in a Schlenk tube, dried in vacuum followed by backfilling with argon. A solution of bis[2-(2-bromoisobutyryloxy) undecyl] disulfide (DTBU) (36 mg, 0.05 mmol) in dry ethanol (10 mL) was added to form the initial attachment layer. After incubation for 3 d at 4 °C, the films were cleaned with ethanol and dried in an argon stream.

The initiator-functionalized gold substrate was placed in a Schlenk tube and dried in vacuum. The flask was refilled with argon prior to the addition of 2-bromoisobutyric tert-butylester (*t* BbiB) (15 µL, 0.08 mmol). In a second dried Schlenk tube, a solution of NIPAM monomer (2.26 g, 19.97 mmol) in a mixture of methanol (7 mL) and ultrapure water (3 mL) is degassed. After backfilling with argon, Cu(I)Br (29 mg, 0.20 mmol) and *N*,*N*,*N*′,*N*″,*N*″-pentamethyldiethylenetriamine (PMDETA) (55 µL, 0.26 mmol) were added. The monomer solution was transferred to the reaction tube using a syringe. After 3 h the substrate was removed, cleaned with methanol, ethanol, and water, and dried in an argon stream. The dry film thickness was determined to be around 70 ± 5 nm with ellipsometry (α-SE) (Figure S1, Supporting Information). Au nanoparticles with different sizes were subsequently drop-cast onto the pNIPAM/Au substrate to reach the final plasmonic nanoconstructs.

Characterization: The samples were monitored in a dark-field microscope (BX51, Olympus) connected to a fiber-coupled spectrometer (QE65000, Ocean Optics), while heating and cooling were controlled by a Linkam stage. The temperature was initially changed from 25 °C to 35 °C at a rate of 5 °C min^{-1}. A single-mode fiber-coupled 637 nm continuous wave laser was coupled into the BX51 for rapid photothermal tuning of individual NPoMs and measurement of the response speed. To obtain enough scattered light to measure the fast response from a single nanoparticle while spectrally filtering out the excitation laser, a more elongated nanoparticle was used to provide a longer-wavelength resonance. A series of neutral density (ND) filters (*ND* = 0.1, 0.2, 0.3, 0.5, 1, 2, 3) was used to tune the laser power, which was calibrated *in situ* with a laser power meter (PM121D, Thorlabs). Edge- (Chroma ET655LP) and passband- (Chroma Z658/10X) filters were used to cut the short-wavelength laser scatter from the spectra. Rapid square-wave laser modulation of the diode laser up to 11 kHz was used to generate short irradiation rise and fall times, and an IR photomultiplier responded to all the resulting light between 680 and 930 nm to track the scattering

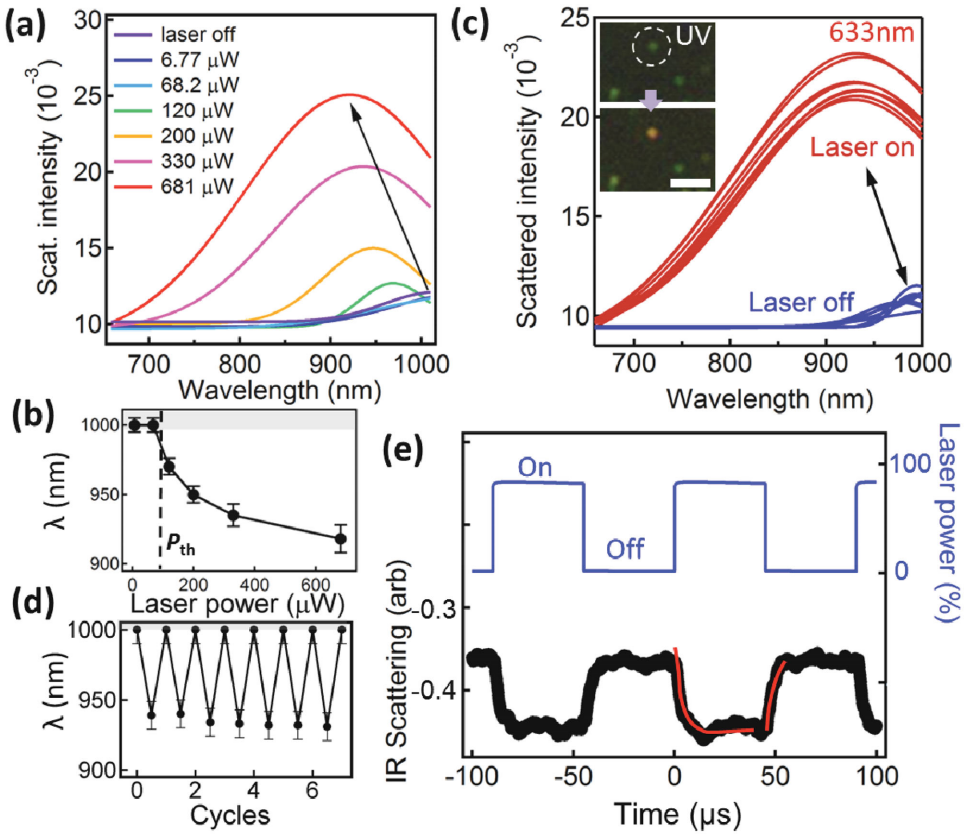

Figure 4. Selective photothermal heating of single Au NPoM with 637 nm laser. a) Power-dependent scattering spectra, and b) extracted peak wavelengths. c) Scattering spectra when irradiating with 0.33 mW, cycled repeatedly on and off. Inset shows change of the NPoM color after irradiation with UV laser, scale bar 2 μm. d) Extracted wavelength changes over six cycles. e) Integrated infrared scattering response of Au NPoM switched with 0.4 mW modulated laser (blue).

changes from the single NPoM (see the setup Figure S10, Supporting Information). The surface morphology of the Au NP on pNIPAM/Au was characterized with scanning electron microscopy (1530VP, Zeiss).

Simulations: Numerical simulations were generated using the volume integral equation in the dipole limit (see the Supporting Information). The dielectric functions were taken from Johnson and Christy.[34] Since the variation in the pNIPAM dielectric constant (changing from 1.33 to 1.40) is small,[35] in all the simulations we consider only dielectric and metallic half-spaces. A broadband plane wave source (from 400 to 1000 nm) was injected in the *xz* plane at 60° with respect to the vertical axis. The excitation includes both *s*- and *p*- polarizations, and a cone 20° around the normal collects the scattered power.

Supporting Information

Supporting Information is available from the Wiley Online Library or from the author.

Acknowledgements

J.J.B. and T.D. conceived the idea, C.R. and M.G. synthesized the PNIPAM films, T.D. fabricated the samples, characterized the films, and measured the spectra. X.Z. and J.J.B. performed calculations and simulations. T.D., F.B., J.J.B., and H.O. performed dynamic irradiation measurements. All authors contributed to this work. This research was supported by UK Engineering and Physical Sciences Research Council grants EP/G060649/1 and EP/L027151/1, and ERC grant LINASS 320503. F.B. thanks the supports from the Winton Programme for the Physics of Sustainability.

Received: February 16, 2016
Published online: March 16, 2016

[1] N. J. Halas, S. Lal, W.-S. Chang, S. Link, P. Nordlander, *Chem. Rev.* **2011**, *111*, 3913.
[2] G. Baffou, R. Quidant, *Chem. Soc. Rev.* **2014**, *43*, 3898.
[3] K. Ueno, H. Misawa, *NPG Asia Mater.* **2013**, *5*, e61.
[4] Y. J. Liu, G. Y. Si, E. S. P. Leong, N. Xiang, A. J. Danner, J. H. Teng, *Adv. Mater.* **2012**, *24*, OP131.
[5] A. E. Cetin, A. Mertiri, M. Huang, S. Erramilli, H. Altug, *Adv. Opt. Mater.* **2013**, *1*, 915.
[6] V. V. Thacker, L. O. Herrmann, D. O. Sigle, T. Zhang, T. Liedl, J. J. Baumberg, U. F. Keyser, *Nat. Commun.* **2014**, *5*, 3448.
[7] X. Shen, C. Song, J. Wang, D. Shi, Z. Wang, N. Liu, B. Ding, *J. Am. Chem. Soc.* **2012**, *134*, 146.
[8] S. J. Tan, M. J. Campolongo, D. Luo, W. Cheng, *Nat. Nanotechnol.* **2011**, *6*, 268.
[9] F. Huang, J. J. Baumberg, *Nano Lett.* **2010**, *10*, 1787.
[10] R. M. Cole, S. Mahajan, J. J. Baumberg, *Appl. Phys. Lett.* **2009**, *95*, 154103.
[11] W. Lewandowski, M. Fruhnert, J. Mieczkowski, C. Rockstuhl, E. Górecka, *Nat. Commun.* **2015**, *6*, 6590.

[12] S. Z. Nergiz, S. Singamaneni, *ACS Appl. Mater. Interfaces* **2011**, *3*, 945.
[13] Y. Lu, G. L. Liu, L. P. Lee, *Nano Lett.* **2005**, *5*, 5.
[14] J.-E. Lee, K. Chung, J. Lee, K. Shin, D. H. Kim, *Adv. Funct. Mater.* **2015**, *25*, 6716.
[15] J. Kim, H. Son, D. J. Cho, B. Geng, W. Regan, S. Shi, K. Kim, A. Zettl, Y.-R. Shen, F. Wang, *Nano Lett.* **2012**, *12*, 5598.
[16] T. A. F. König, P. A. Ledin, J. Kerszulis, M. A. Mahmoud, M. A. El-Sayed, J. R. Reynolds, V. V. Tsukruk, *ACS Nano* **2014**, *8*, 6182.
[17] T. Ding, J. Mertens, D. O. Sigle, J. J. Baumberg, *Adv. Mater.* **2015**, *27*, 6457.
[18] T. Ding, D. Sigle, L. Zhang, J. Mertens, B. de Nijs, J. Baumberg, *ACS Nano* **2015**, *9*, 6110.
[19] M. A. Ward, T. K. Georgiou, *Polymers* **2011**, *3*, 1215.
[20] Y. Guan, Y. Zhang, *Soft Matter* **2011**, *7*, 6375.
[21] M. Karg, I. Pastoriza-Santos, J. Pérez-Juste, T. Hellweg, L. M. Liz-Marzán, *Small* **2007**, *3*, 1222.
[22] C. Fernández-López, L. Polavarapu, D. M. Solís, J. M. Taboada, F. Obelleiro, R. Contreras-Cáceres, I. Pastoriza-Santos, J. Pérez-Juste, *ACS Appl. Mater. Interfaces* **2015**, *7*, 12530.
[23] A. C. Manikas, G. Romeo, A. Papa, P. A. Netti, *Langmuir* **2014**, *30*, 3869.
[24] Y. Wu, F. Zhou, L. Yang, J. Liu, *Chem. Commun.* **2013**, *49*, 5025.
[25] D. Fava, M. A. Winnik, E. Kumacheva, *Chem. Commun.* **2009**, 2571.
[26] M. Karg, T. Hellweg, P. Mulvaney, *Adv. Funct. Mater.* **2011**, *21*, 4668.
[27] S. Christau, T. Möller, Z. Yenice, J. Genzer, R. von Klitzing, *Langmuir* **2014**, *30*, 13033.
[28] J. Mertens, A. L. Eiden, D. O. Sigle, F. Huang, A. Lombardo, Z. Sun, R. S. Sundaram, A. Colli, C. Tserkezis, J. Aizpurua, S. Milana, A. C. Ferrari, J. J. Baumberg, *Nano Lett.* **2013**, *13*, 5033.
[29] B. C. Choi, S. Choi, D. E. Leckband, *Langmuir* **2013**, *29*, 5841.
[30] R. W. Taylor, T.-C. Lee, O. A. Scherman, R. Esteban, J. Aizpurua, F. M. Huang, J. J. Baumberg, S. Mahajan, *ACS Nano* **2011**, *5*, 3878.
[31] L.-W. Xia, R. Xie, X.-J. Ju, W. Wang, Q. Chen, L.-Y. Chu, *Nat. Commun.* **2013**, *4*, 2226.
[32] J. R. Morones, W. Frey, *J. Nanopart. Res.* **2010**, *12*, 1401.
[33] O. M. Wilson, X. Hu, D. G. Cahill, P. V. Braun, *Phys. Rev. B* **2002**, *66*, 224301.
[34] P. B. Johnson, R. W. Christy, *Phys. Rev. B* **1972**, *6*, 4370.
[35] W. G. Brett, C. Tong, G. Santaneel, H. Zhibing, N. Arup, *Appl. Phys. Express* **2009**, *2*, 057001.